WATER RESOURCES RESEARCH

Volume 48 | Number 12 | December 2012
Articles published online 1 December - 31 December 2012

AGU PUBLISHED BY THE AMERICAN GEOPHYSICAL UNION

Coupling the snow thermodynamic model SNOWPACK with the microwave emission model of layered snowpacks for subarctic and arctic snow water equivalent retrievals

A. Langlois,[1] A. Royer,[1] C. Derksen,[2] B. Montpetit,[1] F. Dupont,[3] and K. Goïta[1]

Received 14 March 2012; revised 6 November 2012; accepted 7 November 2012; published 20 December 2012.

[1] Satellite-passive microwave remote sensing has been extensively used to estimate snow water equivalent (SWE) in northern regions. Although passive microwave sensors operate independent of solar illumination and the lower frequencies are independent of atmospheric conditions, the coarse spatial resolution introduces uncertainties to SWE retrievals due to the surface heterogeneity within individual pixels. In this article, we investigate the coupling of a thermodynamic multilayered snow model with a passive microwave emission model. Results show that the snow model itself provides poor SWE simulations when compared to field measurements from two major field campaigns. Coupling the snow and microwave emission models with successive iterations to correct the influence of snow grain size and density significantly improves SWE simulations. This method was further validated using an additional independent data set, which also showed significant improvement using the two-step iteration method compared to standalone simulations with the snow model.

Citation: Langlois, A., A. Royer, C. Derksen, B. Montpetit, F. Dupont, and K. Goïta (2012), Coupling the snow thermodynamic model SNOWPACK with the microwave emission model of layered snowpacks for subarctic and arctic snow water equivalent retrievals, *Water Resour. Res.*, *48*, W12524, doi:10.1029/2012WR012133.

1. Introduction

[2] Seasonal snow cover plays an important role in the surface energy balance [e.g., *Male and Granger*, 1981; *Arons and Colbeck*, 1995; *Gustafsson et al.*, 2001] through its high albedo, low thermal conductivity, and diffusivity [e.g., *Li and Zhou*, 2001; *Albert*, 2002; *Lemke et al.*, 2007]. Furthermore, snow is a key hydrological variable, acting as an important freshwater reservoir [e.g., *Barnett et al.*, 2005], necessary for the health of ecosystems and energy production (e.g., hydroelectricity). Variability in snow melt and snow melt timing has major implications for permafrost regimes [*Romanovsky et al.*, 2010] and associated geochemical cycling.

[3] Large uncertainties remain with regard to the effect of snow on climatological cooling and heating patterns [*Fletcher et al.*, 2009]. Furthermore, the lack of proper snow depth and snow water equivalent (SWE) information within global circulation models lead to uncertainties in climate predictions [*Essery*, 1998; *Brown et al.*, 2003; *Hardiman et al.*, 2008; *Dutra et al.*, 2010]. The uncertainties are larger in northern latitudes where the observed warming is strongest [i.e., *Kaufman et al.*, 2009] due to a lack of in situ snow and meteorological observations used to drive the models. A realistic representation of snow (e.g., SWE) is therefore imperative to make reliable projections about the response of the northern environment to a warming climate. This was addressed in numerous studies using various remote sensing methods to monitor snow cover extent using visible-near infrared remote sensing [e.g., *Hall et al.*, 1995; *Maurer et al.*, 2003; *Salomonson and Appel*, 2004; *Frei and Lee*, 2010]. However, those methods do not allow the retrieval of SWE, a crucial parameter related to cryospheric energy and water budgets. The use of spaceborne passive microwave measurements has proven to be a useful tool in determining SWE over land [e.g., *Chang et al.*, 1982; *Foster et al.*, 1997; *Pulliainen and Hallikainen*, 2001; *Derksen et al.*, 2005, 2010] and sea ice [e.g., *Markus and Cavalieri*, 2000; *Langlois et al.*, 2007, 2010a], but the satellite sensor coarse spatial resolution ($\sim$625 km^2) combined with high spatial variability of snow and vegetation properties [e.g., *Foster et al.*, 2005; *Langlois et al.*, 2011] introduces random and systematic uncertainties that can produce high error values for retrieval methods that rely solely on passive microwave measurements.

[4] Recently, multilayered thermodynamic snow models such as SNOWPACK [*Bartelt and Lehning*, 2002] have demonstrated potential in SWE predictions [e.g., *Langlois et al.*, 2009]. The coupling of such models with climatological

[1]Centre d'Applications et de Recherches en Télédétection, Université de Sherbrooke, Sherbrooke, Québec, Canada.
[2]Climate Research Division, Environment Canada, Toronto, Ontario, Canada.
[3]Laboratoire de Glaciologie et Géophysique de l'Environnement (LGGE) UMR 5183, UJF—Grenoble 1/CNRS, Grenoble, France.

Corresponding author: A. Langlois, Département de Géomatique Appliquée, Centre d'Applications et de Recherches en Télédétection (CARTEL), Université de Sherbrooke, Office A4-280, Sherbrooke, Québec J1K 2R1, Canada. (a.langlois2@usherbrooke.ca)

0043-1397/12/2012WR012133

reanalysis data such as the North American Regional Reanalysis (NARR) showed reasonable SWE predictions in northeastern Canada, and the use of reanalysis data to drive snow models can address the spatial limitations of driving the model with meteorological observations, given the sparse spatial coverage of stations across Canada (about 25 stations per 100,000 km^2; *Metcalfe and Goodison* [1993]). Modeled snow information coupled with passive microwave radiative transfer models such as the microwave emission model of layered snowpacks (MEMLS) [*Wiesmann and Mätzler*, 1999] could further improve our understanding of retrieval accuracy and hence regional SWE variability.

[5] Recent work using passive microwave data has shown potential in retrieving SWE [*Andreadis and Lettenmaier*, 2006; *Pulliainen*, 2006; *Pardé et al.*, 2007; *Durand and Margulis*, 2007; *Touré et al.*, 2011; *Takala et al.*, 2011]. However, most iteration procedures using passive microwave data are conducted solely on SWE, while large uncertainties still remain with regard to snow grain size parameterization. Grain size is by far the most significant variable affecting radiative transfer in the microwave models and yet is ignored or simply treated in recent studies. Those large uncertainties could lead to bias in SWE retrievals such as systematic overestimation or underestimation, by compensating for errors due to poor snow grain parameterization through SWE. Thus, it becomes necessary to assess the retrieval of snow grain size information in current models, which is hampered by a lack of field measurements arising from sampling constraints. Some of the literature suggests that "grain size" is poorly defined and measured with repeatability problems [e.g., *Domine et al.*, 2006]. Since the morphology is extremely variable and can change in a matter of hours [e.g., *Colbeck*, 1983; *Arons and Colbeck*, 1995; *Domine et al.*, 2008; *Langlois et al.*, 2008], validation of such models with accurate field measurements is yet to be done. Of particular relevance, most SWE algorithms make use of passive microwave radiative transfer principles, where large uncertainties are related to the poor definition of snow grain size profiles [e.g., *Grenfell and Warren*, 1999; *Mätzler and Wiesmann*, 1999; *Roy et al.*, 2004; *Foster et al.*, 2005]. In fact, it was shown using various radiative transfer models such as MEMLS [*Durand et al.*, 2008; *Langlois et al.*, 2010a], Helsinki University of Technology [*Butt and Kelly*, 2008; *Kontu and Pulliainen*, 2010; *Derksen et al.*, 2012a], and Dense Media Radiative Transfer (DMRT) [*Tedesco and Kim*, 2006; *Grody*, 2008; *Brucker et al.*, 2010] that simulated T_b are very sensitive to snow grain size, and yet this variable is poorly characterized. Promising results from various methods show that near-infrared reflectance can be linked to specific surface area of snow grains [*Matzl and Schneebeli*, 2006; *Domine* et al., 2006; *Picard et al.*, 2010; *Langlois et al.*, 2010b]. Results from those methods, along with the coupling of a snow and microwave emission model, would allow an improved assessment of the snow grain information from snow model, with related uncertainties, and a more accurate retrieval of snow variables such as SWE.

[6] While satellite microwave brightness temperatures exhibit strong sensitivity to the scattering properties of terrestrial snow, SWE retrieval solutions based solely on empirical relationships between microwave brightness temperature and SWE still perform poorly. Data iteration approaches, however, that can include a physical snowpack model coupled with a radiative transfer scheme are a possible solution [*Durand et al.*, 2008]. With this goal in mind, the present study evaluates the feasibility of driving a physical snowpack model (SNOWPACK) with the NARR, the outputs of which will be coupled with the MEMLS. The model SNOWPACK is appropriate, since it produces detailed snowpack information far beyond bulk properties like density, depth, and SWE. Radiometric models require stratigraphy and grain size information that are produced by this model. Hence, our main objective is to reduce the uncertainties in SWE simulated by snow models by incorporating passive microwave observations within an iterative scheme (i.e., iteration until error is minimized), which is completely independent from field measurements. Specifically, we want to (a) couple the thermodynamic multilayer snow model (SNOWPACK) to MEMLS, (b) quantify and correct the uncertainty related to poor snow grain information initially predicted by SNOWPACK, and (c) to correct modeled SWE from SNOWPACK-MEMLS and measured in situ/airborne brightness temperature data.

2. Data and Methods

2.1. International Polar Year and Cold Regions Hydrology High-Resolution Observatory Field Campaigns

[7] Data for this study were collected during two intensive Canadian field campaigns, namely the Canadian International Polar Year (IPY) project "Variability and Change in the Canadian Cryosphere," which took place in northern Québec in February of 2008, and the Canadian Cold Regions Hydrology High-resolution Observatory (CoReH2O) Snow and Ice Experiment throughout the winter 2009–2010 in Churchill (CH), Manitoba.

[8] The IPY intensive field campaign took place in February 2008 and included four high-resolution sampling sites located at Sept-Îles (SI—boreal: 50.3N–66.3W), Schefferville (SC—taiga: 54.8N–66.7W), Kuujjuaq (KU—taiga and tundra: 58.1N–68.6W), and Puvirnituq (POV—open tundra: 59.8N–76.4W), and five flight lines for airborne measurements (Figure 1). At the high-resolution sampling sites, snow and vegetation properties were measured every kilometer within a grid of 8 km × 16 km. Airborne passive microwave measurements along the flight lines were acquired from a Twin Otter equipped with radiometers at 19 and 37 GHz (both horizontal and vertical polarizations). A helicopter crew measured snow and vegetation properties every 40 km between SI and Kangirsuk (KG—open tundra). This ~2000 km transect spanned the transition in vegetation from dense boreal forest to open tundra (Figure 1). More details on the measurement campaign can be found in *Langlois et al.* [2010a, 2011].

[9] The CoReH2O campaign took place between November 2009 and May 2010 in CH, Manitoba [*Derksen et al.*, 2012b] (Figure 1), during which spatially intensive and temporally extensive observation periods were conducted. The data used in this article were collected during four intensive observation periods (IOPs) of 2–3 weeks in January (IOP 1), February (IOP 2), March (IOP 3), and April/May (IOP 4) 2010. Throughout these periods, sites were revisited to capture the temporal evolution of snow physical properties, and their impact on passive microwave

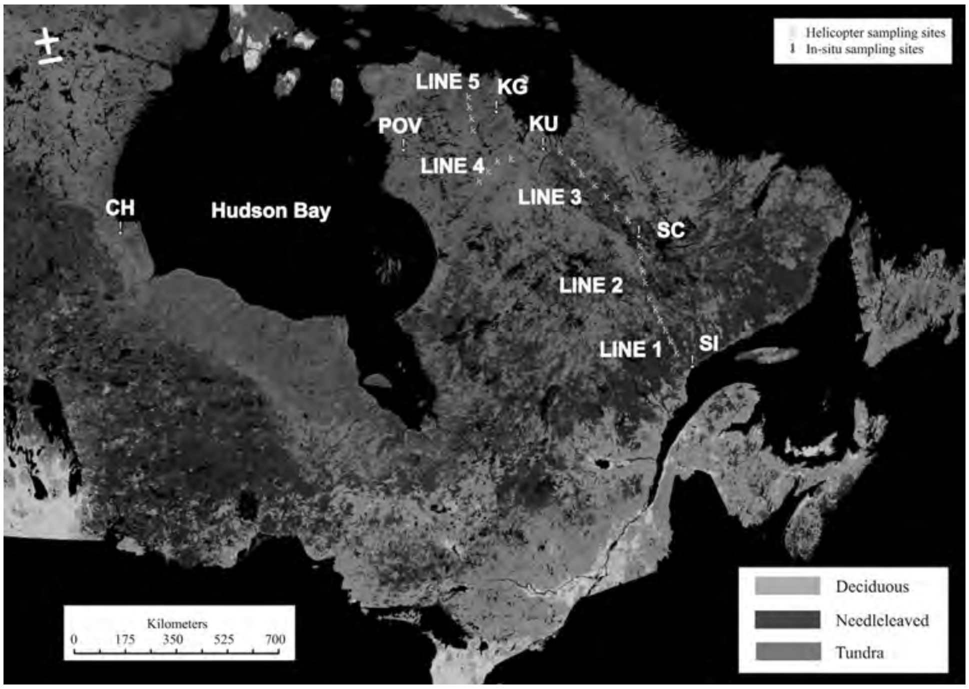

Figure 1. Location of the IPY and CoReH2O field campaign flight lines and sampling sites. The background map is derived from the MODIS land cover product with aggregated classes for clarity.

brightness temperatures measured with sled-based radiometers over various surfaces (clearing in a forested stand, dry/wet fen, and lake ice).

2.2. Snow Properties

[10] Snowpits were dug at each site such that direct solar illumination of the snow wall was avoided. Layered density profiles were obtained by extracting snow samples at 3 cm intervals from the surface to the snow/soil interface using a 192 cm^3 density cutter and weighed using a Pesola light series scale ($\pm$0.5 g). Bulk SWE and density were measured from a snow core at each site. Density was also determined from the product of measured layer density and thickness through each snowpit. Temperature profiles were measured at 3 cm intervals using a Traceable 2000 digital temperature probe ($\pm$0.1°C). The number of sampled sites is given in Table 1.

[11] Snow grain size, a critical parameter strongly affecting microwave snow emission [e.g., *Mätzler*, 1987], was measured (in CH only) using the shortwave InfraRed Integrating Sphere (IRIS) system, similar to the one developed by *Gallet et al.* [2009], which uses an integrating sphere (Labsphere®, 10cm diameter) mounted with two ports on the equator of the sphere at 0° and 90° and one port at the top. The first port located on the equator of the sphere is for the illumination source from a 1.3 μm laser with a 1 cm beam expander. The second port on the equator of the sphere is located in front of the laser and placed in front of the target (snow sample) and the third one at 90° is for an InGaAs photodiode detector. A diaphragm is put in front of the laser beam to measure the dark current and possible parasitic light coming into the sphere. Subtracting the dark current and parasitic light from the measured signal of the sample without the diaphragm allows the clean measurement of the signal reflected by the snow sample. The IRIS system is calibrated to albedo for each snowpit using reference Spectralon targets (0.06, 0.25, 0.59, 0.79, and 0.99 at 1300 nm), taking into account any possible shift in the laser illumination between every snowpit measurement. For more details on the IRIS system, please refer to *Montpetit et al.* [2011] or *Gallet et al.* [2010].

2.3. Moderate Resolution Imaging Spectroradiometer Vegetation Product and Passive Microwave Measurements

[12] Only vegetation-free (forest fraction, $F = 0$) airborne brightness temperatures were used in this study. To identify which sampling sites had available T_b where $F = 0$, we used satellite-derived land cover type and forest fraction maps. The land cover type was determined from the Land Cover Map of Canada 2005, produced by the Canadian Center for Remote Sensing (Natural Resources Canada, Ottawa, Canada) [*Latifovic et al.*, 2004]. The data set encompasses land cover at 250 m spatial resolution, including water fraction. As for the vegetation fraction, values were extracted from the Moderate Resolution Imaging Spectroradiometer (MODIS) vegetation continuous fields available from the Global Land Cover Facility [*Hansen et al.*, 2002]. The vegetation continuous field collection

Table 1. Sampling Sites for the IPY and CoReH2O Campaigns Where T_b, Snow, and Vegetation Properties Data Are Available

Data Set	Dominant Land Cover	Number of Sampling Sites
IPY	Dense boreal forest, taiga, and open tundra	36
CoReH2O	Taiga; open wetland	16

contains proportional estimates for vegetative cover types gathered into three general classes: woody vegetation (forest), herbaceous vegetation, and bare ground.

[13] For the airborne passive microwave measurements, the radiometers were mounted on the National Research Council Twin Otter aircraft, which is described in detail by *Walker et al.* [2002]. The airborne radiometers were precalibrated and postcalibrated each flight using warm (ambient temperature microwave absorber) and cold (liquid nitrogen) targets as described by *Solheim* [1993] and *Asmus and Grant* [1999]. Uncertainty in the measurement of the calibration target temperature was estimated at ± 2 K. The 19 and 37 GHz radiometers were calibrated simultaneously, so the same target temperature uncertainties for a given calibration apply to both frequencies. Estimates of intercalibration receiver drift were made by examining the preflight and postflight calibration target brightness temperatures. Radiometer stability depended on frequency, but overall uncertainty was estimated at ± 2 K at 19 GHz and <1 K at 37 GHz. The aircraft flew over the high-resolution grids at an altitude of 914 m, while the sites sampled by helicopter access were flown at an altitude of 305 m. The ground field of view at 53° incidence angle was approximately 290 m $\times$ 490 m and 120 m $\times$ 200 m for the two altitudes, respectively. One should note that the sites used in this article (Table 1) showed no evidence of melt and contained no ice lenses. The presence of ice lenses complicates MEMLS simulations [*Rees et al.*, 2010], and thus sites where ice was present were removed from the data set. The surface-based measurements conducted in CH used the same set of radiometers mounted on a sled and pulled by a snowmobile. The radiometers were also precalibrated and postcalibrated using warm and cold targets everyday for the duration of the campaign [*Derksen et al.*, 2012b].

2.4. Models

2.4.1. SNOWPACK Simulations Driven by NARR

[14] Snow thermodynamic models require meteorological information as input, which are sparse in northern regions. Regional reanalysis data such as the NARR available (1979–present) from the Environmental Modeling Center, National Centers for Environmental Prediction, represent a good alternative and were used to drive SNOWPACK. The horizontal resolution is 0.3° (approximately 32 km) and the temporal resolution is eight times daily (every 3 h). To simulate snow cover evolution, the model requires, at each time step (set every 3 h), mean values of air (2-m) and surface temperatures (°C), relative humidity (%), wind speed ($\mathrm{m{\cdot}s^{-1}}$), incoming/reflected shortwave and incoming longwave radiation ($\mathrm{W{\cdot}m^{-2}}$), and cumulative precipitation over the 3 h period ($\mathrm{kg{\cdot}m^{-2}}$ or mm). A local validation of NARR can be found in *Langlois et al.* [2009], which found that basic meteorological parameters (temperature, humidity, radiation) are fairly well simulated in southern Québec and that promising results are found in northern regions such as KU and SC; however, further investigation is required with regard to precipitation. Thermophysical processes of interest in SWE studies such as phase change, water vapor transport (i.e., metamorphism), and loss (runoff, evaporation, and sublimation) are included within SNOWPACK. The details on the internal models will not be given here; they can be found elsewhere [*Lehning et al.*, 2002; *Bartelt and Lehning*, 2002].

[15] Model settings were specified, given the input data availability mentioned above. Two main types of output data can be visualized through user-friendly software, namely scalar and vector data [*Spreitzhofer et al.*, 2004]. The scalar data are related to individual layers of the snowpack such as the simulated vertical profiles of snow density, temperature, grain size, and shape, whereas vector data are attributed to snow cover evolution, such as depth and SWE. The amount of layers varies, given the number of precipitation events and the predicted snow depth. The transition between solid and liquid precipitation occurs at $+1.2$°C.

2.4.2. Microwave Emission Model of Layered Snowpacks

[16] The MEMLS can be used in the frequency range between 5 and 100 GHz [*Mätzler and Wiesmann*, 1999; *Wiesmann and Mätzler*, 1999]. The model is based on radiative transfer theory, which allows the scattering coefficient to be predicted from physical snow parameters and the absorption coefficient from dielectric properties of ice. Snow cover is considered as a series of horizontal layers (L) each characterized by thickness, reflectivity (r_L), emissivity (e_L), transmissivity (t_L), and temperature (T_L). The model automatically computes these parameters using snow information as input. To obtain accurate characterizations of r_L, e_L, and t_L, a six-flux three-dimensional approach is used within each layer. The horizontal fluxes represent radiation that is trapped in the snow cover and cannot exit at incidence angles (θ) larger than the critical angle θ_c. The vertical fluxes represent the radiation that escapes the snow cover at $\theta < \theta_c$. Further details on the radiation transfer theory used in MEMLS can be found in *Mätzler and Wiesmann* [1999] and *Wiesmann and Mätzler* [1999]. The primary input profile data are density (ρ_s), snow temperature (T_s), liquid water content (W_s), correlation length (l_c), vertical extent (z_L), physical ground temperature (T_g), and snow-ground interface reflectivity (r_0), which were derived through the NARR-SNOWPACK coupling and field observations. From these primary parameters, the dielectric properties (for dry and wet snow) as well as the absorption (γ_a) and scattering (γ_s) coefficients can be derived. The soil parameters in MEMLS were set using the soil reflectivity model of *Wegmüller and Mätzler* [1999].

2.4.3. Correction of Simulated Snow Grains

[17] The output of the SNOWPACK simulations driven by NARR were used as input to MEMLS. We kept the same number of layers as predicted by SNOWPACK (which were not constrained and so were different for each site, given the variability in the number of precipitation events and the predicted snow thickness), but the snow grain optical diameter values (from SNOWPACK, d_{opt}) were replaced by correlation length values (requested in MEMLS, l_c) such that

$$l_c = \frac{2}{3} \cdot \left(1 - \frac{\rho_{\mathrm{snow}}}{\rho_{\mathrm{ice}}}\right) \cdot d_{\mathrm{opt}}, \quad (1)$$

where ρ_{snow} and ρ_{ice} are, respectively, snow and ice density in $\mathrm{kg{\cdot}m^{-3}}$ [*Mätzler*, 1992a]. Using the NARR forced snow information from SNOWPACK as input to MEMLS, a two-step iteration process for SWE retrieval was developed such that simulated snow grain size was corrected using measured and simulated T_b (first iteration) prior to retrieving SWE (second iteration), also using measured and simulated T_b (Figure 2).

[18] By doing so, we avoid compensation through SWE for poor snow grain parameterization. We compared simulated and measured T_b and applied a correction factor (multiplying factor φ, as depicted in Figure 2) on simulated correlation length (l_c) values until a minimum root-mean-square error (RMSE) was reached. It was demonstrated by *Lundy* [2000] that SNOWPACK is able to predict the trends in density with some degree of accuracy (R^2: 0.83, mean-square error: 66 kg·m^{-3}), but uncertainties are related to incorrect calculation of grain size and bond. Predicting the rate of grain growth during equilibrium and kinetic-growth metamorphism is a complex task, and the physics used by SNOWPACK have not been extensively validated due to the complexity of measuring snow grains properly (lack of reference data). Another possible problem lies in the assignment of the initial grain size of new snow, which is set constant (i.e., standard value). Since the model only allows grain growth, no grain sizes less than this initial value are ever predicted (which leads to systematic overestimation of grain size), leading to low T_b simulations (i.e., through loss due to excessive scattering) and very large RMSE. Snow grain simulations from SNOWPACK [*Huang et al.*, 2012] or other multilayered snow thermodynamic models such as CROCUS were investigated in other studies [*Morin et al.*, 2012; *Brucker et al.*, 2010]. They outline the problem of different definitions of "grain size" and treatment of its growth, leading to the need for adjustment prior to be coupled with a snow emission model. Thus, before focusing on the objective of this study (i.e., retrieve SWE), it appears necessary to show whether the snow model overestimates or underestimates snow grain size when compared to available in situ measurements, using which this bias can be corrected with passive microwave measurements.

3. Results and Discussion

3.1. Snow Properties

[19] We selected sampling sites at which vegetation-free airborne brightness temperatures ($T_{b\text{-SNOW}}$) were available. At each site, SWE was measured and compared to NARR-SNOWPACK runs. Results are highlighted in Table 2 for both IPY and CoReH2O campaigns. The differences between measured and modeled SWE values are highly variable from one site to another, and the relationship between modeled and measured SWE is depicted in Figure 3.

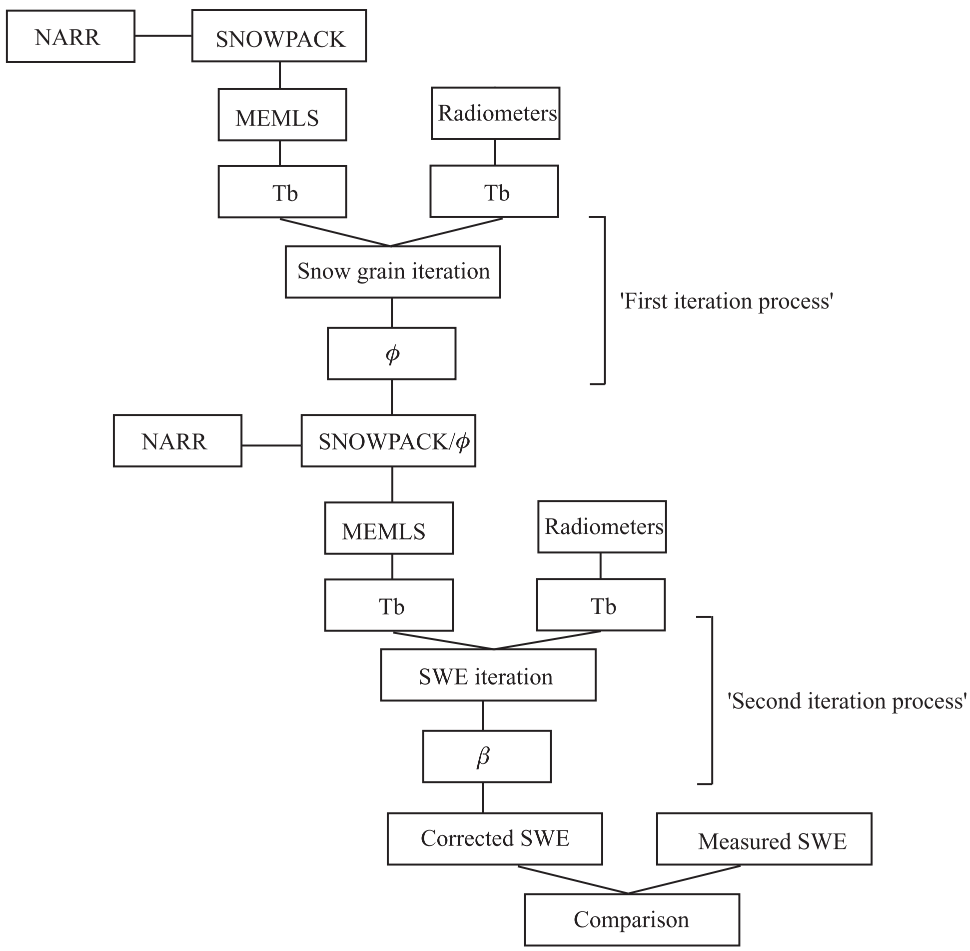

Figure 2. Two-step iteration method using measured and simulated brightness temperatures for predicted snow grain correction and SWE retrieval.

Table 2. Measured and Modeled SWE (NARR-SNOWPACK) for the IPY and CoReH2O Data Sets

		SWE (mm)					
		Measured			SNOWPACK		
Data Set	*n* Sites	Min.	Max.	Avg.	Min.	Max.	Avg.
IPY	36	43.6	450.8	189.2	125.4	256.9	173
CoReH2O	16	56.6	334.2	154.2	81.5	146.7	112.7

[20] The initial SWE predictions from NARR-SNOWPACK (no passive microwave measurements considered) are quite poor with a slope of 0.23, a y-axis intercept (offset) of 108.9 mm of SWE, an RMSE of 79.4 mm, and a mean bias of 26.5 mm. Overall, SNOWPACK largely underestimates SWE, and improving on this result using an iterative scheme to retrieve SWE from measured and modeled passive microwave brightness temperatures is the main objective of this article. It would be difficult to identify the forcing process behind the large modeled underestimation compared to observations. The performance of SNOWPACK in predicting SWE can vary from one site to another and is different from year to year [*Langlois et al.*, 2009]. One of the potential explanations is that local precipitation gauge measurements are highly uncertain in remote northern locations, and systematic biases can be significant [*Yang et al.*, 1999]. Northern areas are usually open, and wind disturbance can be significant, leading to lower catch efficiencies by the gauges (i.e., lower measured precipitation), which, in turn, leads to systematically smaller precipitation values in NARR and hence SWE values in SNOWPACK. This is in agreement with *Langlois et al.* [2009] that found more accurate SWE simulations in southern Québec at a research station with proper maintenance and protected from wind disturbance. Because of its recent release, the strengths and weaknesses of NARR are largely undocumented [*Mesinger et al.*, 2006]. Although NARR provides much improved representation of precipitation when compared to other reanalysis products [*Bukovsky and Karoly*, 2007], *Mesinger* et al. [2006] identified some of the known weaknesses, including precipitation inaccuracies over Canada. Although it is hard to quantify the exact uncertainties in high latitude precipitation data, the work by *Langlois et al.* [2009] has shown reasonable NARR precipitation estimates over seasonal time scales in some areas. Furthermore, Figure 3 clearly shows important variability in measured SWE within one NARR pixel (i.e., one simulated SWE value by SNOWPACK). This variability is explained by different environments in which sampling occurred (fen, forest, open tundra). Hence, changing precipitations would only move the cluster up or down as shown in Figure 3, when clear improvement is needed on the slope. The SWE simulations need to be improved individually at each site (i.e., at the model level) rather than on precipitations that

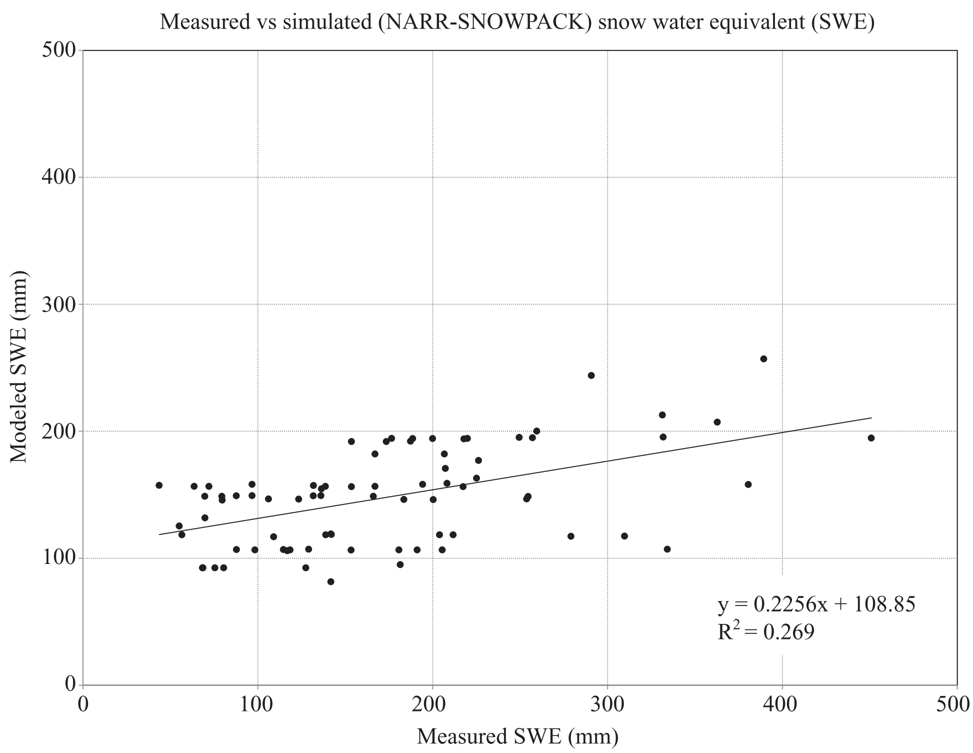

Figure 3. Comparison between initial modeled SWE values from NARR-SNOWPACK (without consideration of passive microwave measurements) and field-measured values.

would logically not improve the above results. Finally, the modeled density values from SNOWPACK are generally underestimated, where the underestimation increases with increasing thickness. This leads to larger underestimation in SWE for deep snow, as discussed in Figure 6. The new snow density is a function of air and surface temperatures (range −12°C to +2°C), wind speed, and relative humidity. The snow density estimations are based on statistical relationships from the Alps, and their applicability to other regions presented in this article needs further evaluation [*Lehning et al.*, 2002].

3.2. Simulated Snow Grain Size Correction

[21] The initial MEMLS T_b with SNOWPACK-derived grain size (no correction) varied between 80 and 150 K, which are unrealistically low values for these conditions. The SNOWPACK l_c values were initially predicted with an average of 0.82 mm, with values up to 1.9 mm. However, it was shown by *Wiesmann et al.* [1998] that typical snow has l_c values ranging between 0.06 mm (new snow) and 0.25 mm (depth hoar), which are much lower than those simulated by SNOWPACK. Hence, the resulting scattering from overestimated l_c values is significant when MEMLS is coupled directly to SNOWPACK.

[22] To address this issue, we coupled snowpit measurements (temperature, density, depth) with simulated (NARR-SNOWPACK) correlation length values and used the data as input to MEMLS to find an optimal scaling coefficient (φ), which provides the lowest RMSE values between simulated and measured T_b. Initial RMSE values (i.e., $\varphi = 1$, no correction on grain size) ranged between 136 and 170 K at 19 and 37 GHz (V and H pol.), as shown in Table 3. The minimum RMSE between simulated (using snowpit information and SNOWPACK l_c predicted values) and measured T_b was obtained with a $\varphi = 0.1$ at all frequencies and polarizations, which produced RMSE values of 7.8, 8.1, 26, and 26.8 K at 19V, 19H, 37V, and 37H, respectively (Table 3). The corrected l_c values (SNOWPACK l_c reduced by ~90%) are closer to what was determined by *Wiesmann et al.* [1998]. Furthermore, the corrected l_c values are in agreement with IRIS measurements conducted in CH (Table 4). The high sensitivity of the IRIS system to grain size under controlled illumination provides improved retrievals of snow grain size information [e.g., *Domine et al.*, 2006; *Montpetit et al.*, 2011]. The reason why IRIS was not used to determine the φ is that the overarching goal is to be completely independent from field measurements (presented in the first iteration process; Figure 2). Nonetheless, l_c values from Table 4 are well below the initial values simulated by SNOWPACK ($\varphi = 1$) but agree quite well with the corrected values using $\varphi = 0.1$ obtained through the T_b iteration. This demonstrates just how important such a correction is, prior to any further iteration.

Table 4. Correlation Length Derived From IRIS Measurements in CH Compared to Scaled SNOWPACK l_c Values

Method	Correlation Length, l_c (mm)		
	Min.	Max.	Average
IRIS (197 measurements)	0.017	0.306	0.161
SNOWPACK l_c–φ	0.020	0.175	0.118

[23] Once the snow grain size information is corrected, the obtained RMSE in the SNOWPACK-MEMLS T_b includes errors related to other snow properties, but primarily to the density because the dielectric constant is largely controlled by density in dry snow conditions [e.g., *Tiuri et al.*, 1984; *Hallikainen et al.*, 1986; *Mätzler*, 1987; *Huining et al.*, 1999]. Hence, some differences in SNOWPACK modeled density were found in the initial runs when compared against field measurements (density generally underestimated by SNOWPACK), which can explain some of the differences between modeled and measured SWE (Figure 3). Hence, these differences were addressed by a second modeling iteration to retrieve SWE (see the flowchart in Figure 2). Assimilating SWE values without prior correction of unrealistic grain size representation would produce heavily biased simulations, so the φ correction factor was included in the SWE iteration. The use of simultaneous (two free variables: grain size and SWE) iteration method as proposed by *Pardé et al.* [2007] leads to larger errors than those proposed here. The successive iteration presented in this article (first snow grain size, then SWE) was already addressed in previous studies using spaceborne data [e.g., *Pulliainen*, 2006], but the results highlighted the difficulty of using such an iteration scheme in mixed pixels (i.e., given the low spatial resolution of passive microwave satellite data, many spatial features contribute to the signal). This constraint is well addressed in this article by using high spatial resolution airborne data with relatively homogeneous pixels.

3.3. SWE Retrievals Using Modeled and Airborne T_b Iteration

3.3.1. SWE Iteration Range

[24] Previous studies have shown that T_b values at 37 GHz typically decrease, as the scattering volume (i.e., SWE) increases, which is the basis behind most SWE algorithms using the difference between 19 and 37 GHz, ΔT_b (a larger ΔT_b due to decreasing brightness temperatures at 37 GHz with increasing snow depth) [e.g., *Chang et al.*, 1982; *Mätzler*, 1987]. However, with large values of SWE, this scattering behavior is no longer evident because the 37 GHz

Table 3. Initial RMSE Values Between Measured and Modeled Brightness Temperatures and Associated Values After φ Correction (Scaling Factor) on l_c Values

Source	φ	RMSE (K)							
		19V		19H		37V		37H	
		Initial	With φ	Initial	With φ	Initial	With φ	Initial	With φ
Snowpit-SNOWPACK	0.1	169.7	7.8	154.9	8.1	146	26	136.2	26.8

brightness temperature increases with higher SWE due to emission from the snowpack itself that masks the large scattering from large depth hoar grains [e.g., *Rosenfeld and Grody*, 2000; *Dong et al.*, 2005] (Figure 4). This reversal from the "classical" ΔT_b pattern can cause ambiguity in SWE retrievals. Hence, to improve the accuracy of the SWE retrieval iteration, we limited consideration to cases where the effect mentioned above was not observed. By looking at the brightness temperature, we found that the reversal slope of the T_b versus SWE relationship occurs at measured SWE values larger than 148 mm (up to a measured maximum of 290 mm). This corresponds to snow depths of 65–105 cm at an average density of 250 kg·m^{-3}. The 148 mm threshold was determined using the minimal T_b values of a second-degree polynomial fit on averaged ranges of SWE with 25 mm increment (which did not show statistical significance).

[25] Obviously, the slope reversal depends upon snow physical properties (i.e., grain size; stratigraphic properties) and dielectric properties that are highly variable spatially and temporally. For instance, *Qiu et al.* [2011] demonstrated that this reversal can be highly dependent on snow grain size where the reversal occurs at relatively deeper snow with small snow grain size values. However, many differences exist between various studies. Most differences arise from the different polarizations (V versus H, with lower penetration depth for H-polarized T_b causing an earlier reversal, as seen in Figure 4). Also, given the environment (boreal, taiga, tundra, sea ice, etc.), large differences in T_b can be measured arising from highly variable dielectric properties, which are governed by density, temperature, and wetness. For instance, *Markus et al.* [2006] simulated a slope reversal using $\Delta T_{b19\text{H-}37\text{H}}$ at about 90 cm of snow depth (SWE of 245 mm for density of 250 kg·m^{-3}), whereas the limit is set at 50 cm (SWE of 140 mm for density of 250 kg·m^{-3}) in *Kelly et al.* [2003]. Using Special Sensor Microwave/Imager (SSM/I) data, *Rosenfeld and*

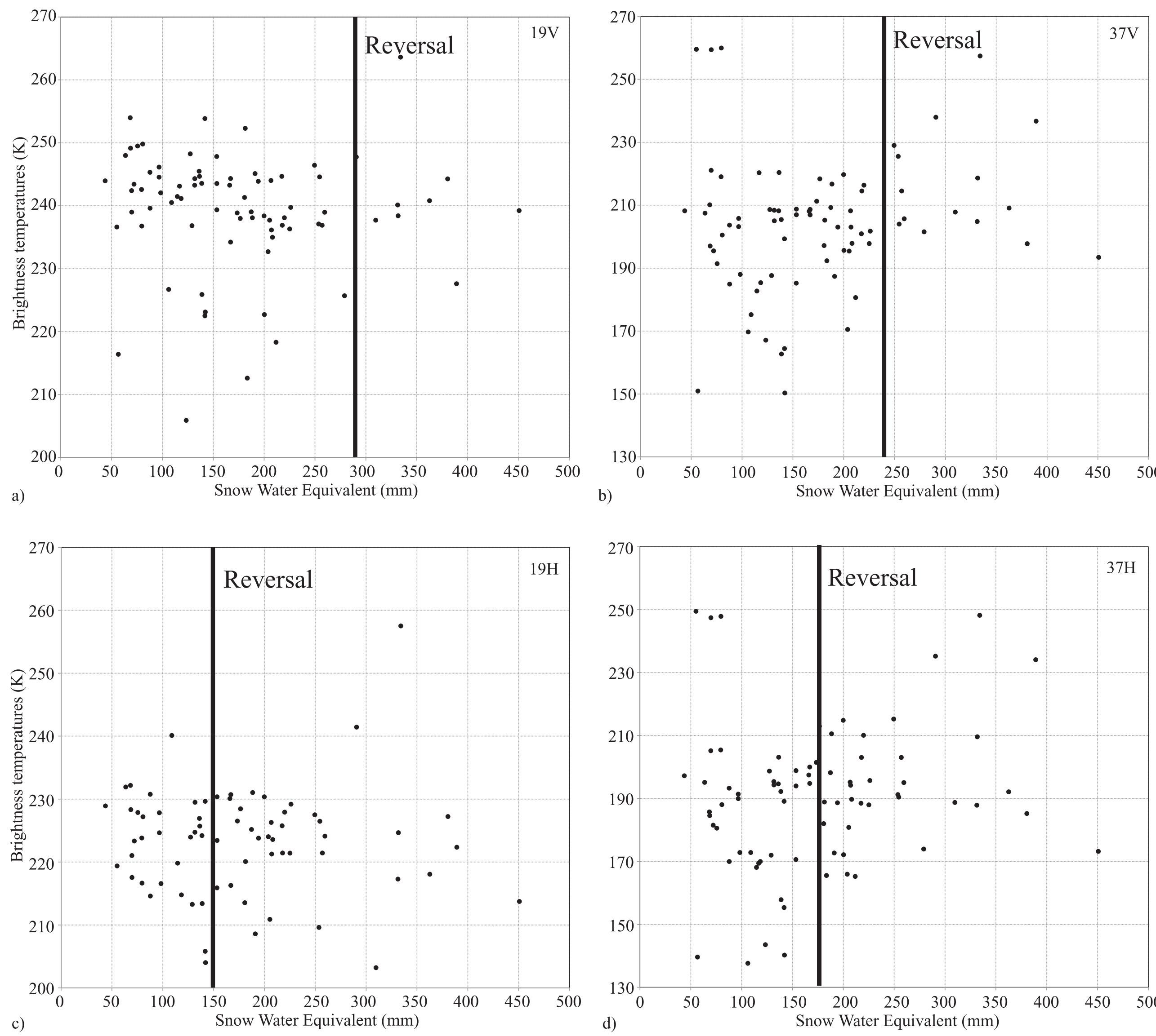

Figure 4. Measured brightness temperature (ground and airborne) as a function of SWE at 19 GHz in the vertical polarization, (a) 19V, (b) 37V, (c) 19H, and (d) 37H. The slope reversal in brightness temperature versus SWE is marked by the bold vertical line.

Grody [2000] observed the reversal at 37V at depths of 40–50 cm. However, one must be careful comparing these findings, since most of evaluations do not take into account vegetation contributions to the signal [e.g., *Kruopis et al.*, 1999; *Pampaloni*, 2004; *Pardé et al.*, 2005; *Lemmetyinen et al.*, 2009; *Langlois et al.*, 2010b, 2011], nor atmospheric effects [e.g., *Kerr and Njoki*, 1990; *Mätzler*, 1992b]. Both effects, which can be neglected in our study since we are using ground and airborne radiometer measurements over vegetation-free areas, can have a significant impact on T_b, leading to a biased slope reversal threshold. In fact, *Derksen* et al. [2010] showed that the reversal occurred at $\sim$130 mm using airborne data, whereas lower SWE threshold was observed using satellite measurements. In light of this, we corrected SWE using measured and modeled brightness temperatures at all frequencies and polarizations, and best results were obtained combining 19V and 37V. From this result, we conducted the second iteration over the 0–290 mm SWE range (290 mm being the limit observed for 19V in Figure 4a).

3.3.2. β Correction Factor for SWE Retrieval

[26] As highlighted in Figure 2, we modified the SNOWPACK-modeled SWE values (using a β factor: when $\beta \mathrm{SWE}_{\mathrm{SNOWPACK}} = \mathrm{SWE}_{\mathrm{measured}}$) using an iterative scheme (minimizing RMSE between observed and modeled T_b by changing SWE values in the input SNOWPACK data) using the snow grain corrected (φ) MEMLS output data from the first iteration process (Figure 2). Two different approaches were tested:

[27] 1. A fixed correction factor, β, was applied to the SNOWPACK-modeled SWE ("β fixed" in Table 5). The β is obtained when the RMSE between measured (radiometer) and simulated (MEMLS) T_b is minimized for all sites combined (i.e., same correction on SWE for each site).

[28] 2. Adjustable β values were computed individually at each site to minimize the difference between $T_{b\text{-rad.}}$ and $T_{b\text{-MEMLS}}$.

[29] From the first approach, the lowest RMSE value on T_b obtained from the iteration was with $\beta = 1.35$ (i.e., modeled SWE values multiplied by 1.35; Figure 5). Although this correction method improves the slope (from 0.23 in Figure 2 to 0.53 in Figure 5), the RMSE (from 79 to 55 mm), and R^2 (from 0.27 to 0.45), the offset increases from 109 to 121 mm, highlighting the need for further improvement.

[30] It appears that the difference between measured and modeled SWE varies with the magnitude of the in situ SWE measurements, which largely explains the poor results in Figure 5. The correlation observed between the measured and modeled SWE differences with the in situ SWE measurements (Figure 6) shows that measured values below 148 mm (corresponding to 148 mm modeled) are lower than predicted values from SNOWPACK. Hence, a more appropriate strategy would be to obtain a β correction factor individually for each site providing the lowest RMSE value between modeled and measured T_b (i.e., SWE value where $T_{b\text{-MEMLS}} \approx T_{b\text{-MEASURED}}$). To establish the reliable range variation of the β correction factor, we computed the optimal β values that would provide the perfect match obtained with $\mathrm{SWE}_{\mathrm{measured}}/\mathrm{SWE}_{\mathrm{SNOWPACK}}$. Those values ranged between 0.4 and 1.9, where values below 1 decrease modeled SWE. We then coupled SNOWPACK and MEMLS using the whole β range (0.4–1.9, step of 0.1) and used the β value as a free parameter that provided the best simulation (i.e., where MEMLS T_b was closest to radiometer measurements).

[31] Since predicted SWE values below 148 mm (value derived from regression in Figure 6) are overestimated by SNOWPACK (Figure 6), their β correction factor should theoretically be $<$1, whereas modeled values over 148 mm should have a $\beta > 1$. Hence, for sites where β values obtained through the iteration did not obey that rule, we simply applied a fixed negative/positive β value ($\beta = 0.7$ for sites that obtained a $\beta > 1$ for SWE < 150 mm, and $\beta = 1.45$ for sites that obtained a $\beta < 1$ for SWE $>$ 148 mm). Such cases can occur under various circumstances of which further analysis is beyond the scope of this article. The forcing values of 0.7 and 1.45 provided the best results, and the obtained corrected modeled SWE values are improved further when compared to a fixed $\beta = 1.35$ (slope, *y*-axis intercept, and R^2) as shown in Figure 7 and Table 5 ("β adjustable" in Table 5).

[32] The relationship between predicted values (with φ and β) shows an improved slope, R^2, and *y*-axis offset and an RMSE of 65.4 mm (Table 5). Thus, the method suggested here improves SWE predictions compared to standalone simulations with a physical snow model driven by regional reanalysis. A similar approach was developed by *Foster et al.* [2011]; however; their approach requires in situ information (not always representative), whereas our methodology is completely independent from surface observations.

3.4. Validation

[33] The method developed above was tested against an independent data set, also acquired during the 2008 IPY campaign near the community of POV (59.8 N–76.45W; see Figure 1). Coincident airborne brightness temperatures and in situ SWE measurements were collected along a transect, spanning two NARR pixels (hence, two NARR-SNOWPACK SWE values). Nearly 5000 snow depths were measured in 5 days, then converted to SWE using average density determined from snow core measurements and were also measured along the snow depth transects (see *Derksen et al.* [2010] for a complete description). The airborne radiometer footprint was about 100 m, within which measured SWE values were averaged (between 10 and 85 SWE measurements in each footprint), leading to a total of 109 points used in the validation.

[34] Obviously, one can expect a poor relationship between NARR-SNOWPACK modeled versus measured SWE (Figure 8a), given that only two modeled SWE values are available and compared against 109 in situ measurements, which were strongly affected by local-scale variability. This is also the reason why no validation was conducted using Advanced Microwave Scanning Radiometer–EOS data. However, for each of the 109 footprints, β values were found using the methodology presented in this article. We

Table 5. Summary of Initial and Corrected SWE Simulation Statistics Compared to Field Measurements

SWE Simulations	Slope	*y*-Axis Offset (mm)	R^2	RMSE (mm)
Initial	0.226	108.85	0.269	79.4
β fixed	0.532	121.13	0.447	54.9
β adjustable	0.891	23.474	0.404	65.4

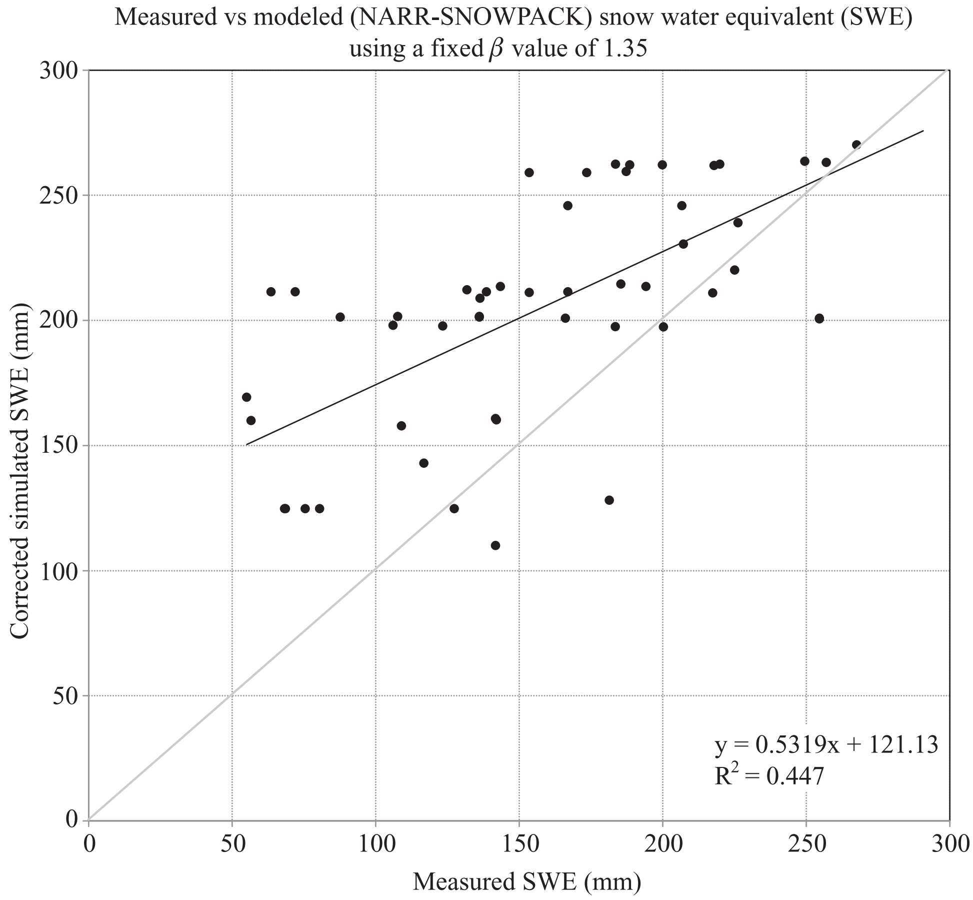

Figure 5. Comparison between modeled SWE values from NARR-SNOWPACK (φ scaling applied to grain size) using a fixed β value of 1.35 (multiplying factor) and measured values.

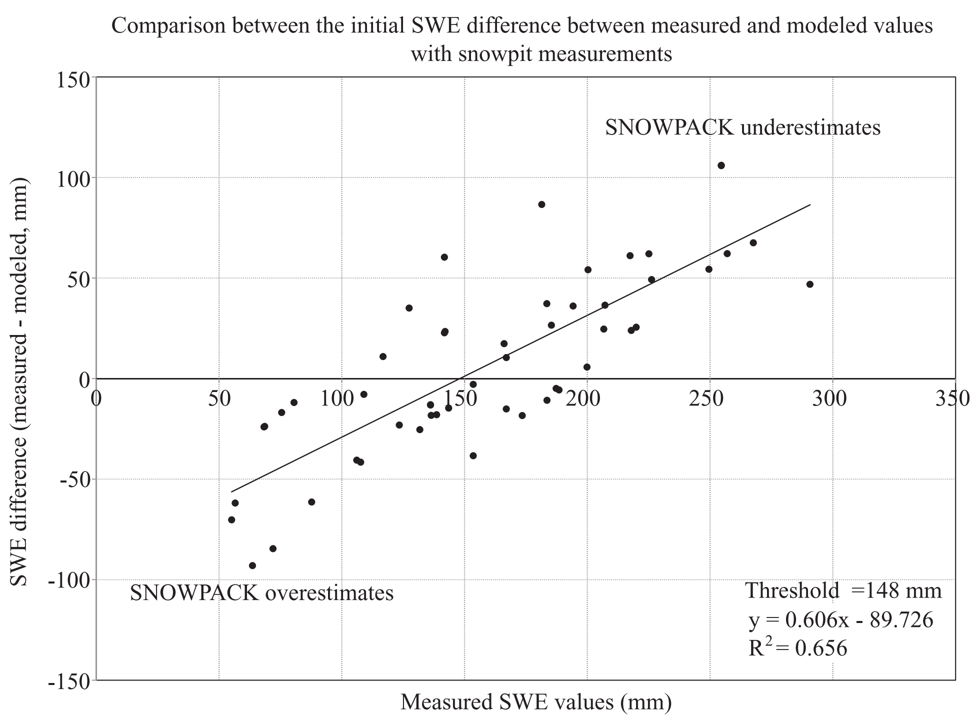

Figure 6. Difference between measured and modeled SWE as a function of measured SWE.

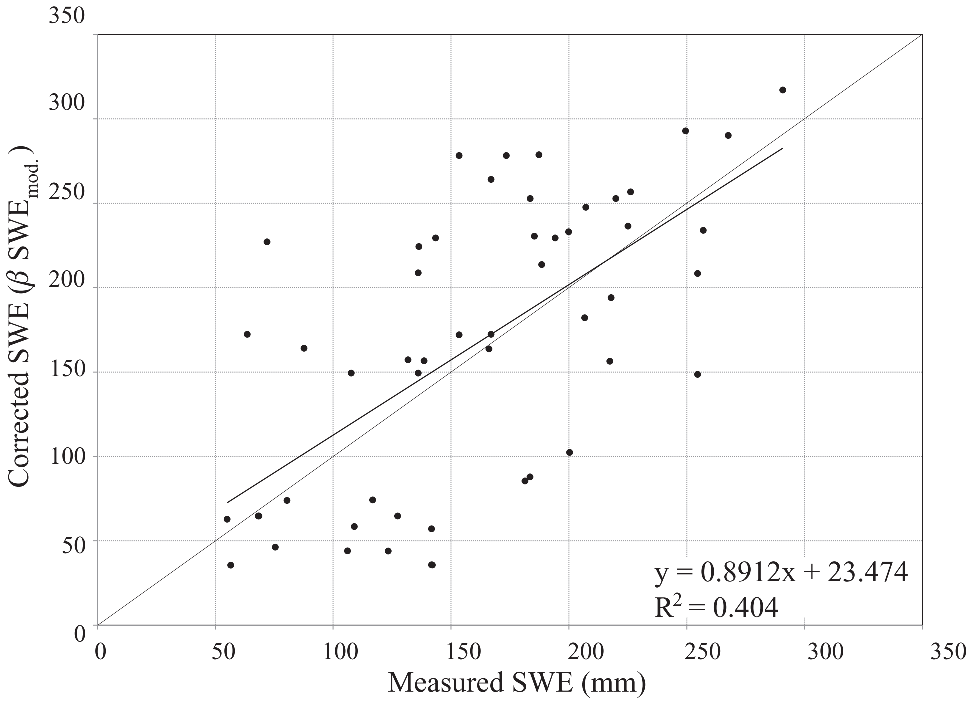

Figure 7. Comparison between modeled SWE values from NARR-SNOWPACK (φ scaling factor applied to grain size) using variable β values (multiplying factor) for each site using a 148 mm threshold (second iteration process, see Figure 2).

retrieved corrected modeled SWE and compared them against field measurements (Figure 8b). Results show that our method clearly improves SWE simulations from SNOWPACK, even with the very high spatial variability measured on the ground. The average standard deviation of measured SWE within the two NARR pixels is 57 mm (min. 14 mm, max. 148 mm).

[35] However, potential sources of error can arise from field measurements of SWE and the inherent spatial variability. Although the latter cannot be corrected but only quantified, it remains a potential source of error. As displayed in Figure 8 for the validation, this spatial variability varied between 14% and 99% within the radiometer footprints (approximately 100 m $\times$ 100 m). *Shook and Gray* [1996] measured the standard deviation of snow depth at sampling distances ranging between 1 m and 1 km and showed that the standard deviation within distances of about 30 m is representative of larger scales [*Clark et al.*, 2011]. However, this specific 30 m spatial variability was not systematically measured on the field and has to be measured in tundra environments. This is crucial to SWE retrievals using coarse spatial resolution passive microwave satellite data and can account for observed biases and explain some of the errors observed in Figures 7 and 8, given the scale differences between snowpit measurements (local) and simulations (NARR-SNOWPACK at $\sim$32 km).

4. Conclusions

[36] We coupled a snow thermodynamic model (SNOWPACK) driven by regional reanalysis data (NARR) with a layered snow emission model (MEMLS) to improve simulations of SWE, completely independent from any surface observations (using the β values from section 3.3.2 considered to be representative). To evaluate the snow model, simulations were compared to in situ measurements from two different field campaigns. We first showed that the initial SWE simulations (without the use of any passive microwave measurements) contained large errors with a regression slope of 0.23 and a y-axis offset of 109 mm. The initial R^2 and RMSE were measured 0.27 and 79 mm, respectively.

[37] To improve this result, we coupled the snow model output to a layered microwave snow emission model. First, the poor grain characterization by the snow model was corrected using an iterative scheme where the simulated snow grain was modified (scaling factor, φ) until a minimum difference in brightness temperatures ($\Delta T_{b\text{-MIN}}$) was found between measured (radiometer) and modeled (MEMLS) data. The most appropriate scaling factor was found to be 0.1 for all sites, which was then applied to the snow model output. The SNOWPACK output data (with corrected snow grain size using φ) was again coupled to MEMLS for a second iteration to retrieve SWE (i.e., modifying SWE until $\Delta T_{b\text{-MIN}}$ was found). A scaling factor for SWE (β) was found for all sites collectively (minimum RMSE) at 1.35. Further improvement occurred when using two β values for underestimated and overestimated SWE values, which produced significant improvement on the slope, y-axis intercept, R^2, and RMSE between modeled SWE (with the two iteratively determined scaling factors) and measured SWE.

[38] It is important to understand that the rather large uncertainties in snow model predictions of SWE and grain size (in our case: SNOWPACK) can be attributed to (1) the model itself and how it treats physical processes such as metamorphism and compaction and (2) the input meteorological

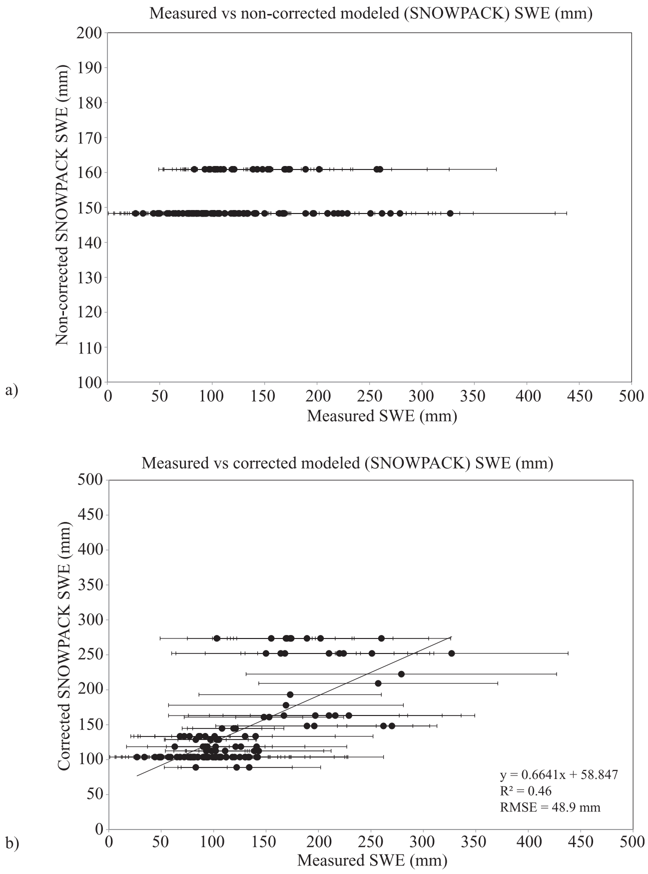

Figure 8. Comparison between modeled and measured SWE (a) before and (b) after the iterations with measured brightness temperatures. Measurements are from transects near the POV (Figure 1). In (a), data span two NARR pixels (therefore, two NARR SWE values). Horizontal lines correspond to the standard deviation of the in situ SWE measurements.

data. It is thus hard to compare and identify key components of the models that are problematic. The overall objective of this article was not to identify and correct weaknesses in SNOWPACK but rather to investigate if T_b can be used to correct initial biases in the snow model whether they come from the model of the input data and without any other source of information on the snowpack. A comparison between similar snow models was conducted in the framework of Snow Model Intercomparison Project (SnowMIP) and by *Langlois et al.* (2009). In this latter analysis, results showed similar biases in three models, namely, SNOWPACK, CROCUS, and SNTHERM. The use of another model performing better in SWE of snow grain simulations would simply change the level of correction needed (φ, β), but the overall improvement would not necessarily change. Improving the physical treatment of SNOWPACK is out of the scope of this study.

[39] Validation using an independent snow survey data set over tundra with strong local-scale variability showed promising results, with a RMSE of 49 mm, and we showed that our method can be applied over a wide range of SWE values (45–260 mm). Furthermore, most studies presented in section 1 are using satellite-passive microwave data, which include T_b contributions from various surface characteristics such as roughness, spatial variation in snow thickness and thermophysical properties, and snow grain size. Hence, the exact nature of each contribution is hard to quantify at the satellite scale and remains poorly studied. The airborne-derived brightness temperatures used in this article are generally more sensitive to plot-scale characteristics, increasing the challenge of SWE retrieval. On the other hand, this increased sensitivity to snow properties allowed the correction for poor grain simulations by the snow model (φ), which represents a step forward for iterative schemes (for future spaceborne retrievals). We showed that coupling a snow thermodynamic model with a microwave snow emission model without accounting for poor grain parameterization uncertainty leads to very large errors, with RMSE $>$100 K in brightness temperatures. A simple two-step iterative procedure (first iteration on snow grains and second on SWE) driven by meteorological reanalysis and without any in situ snow information allows similar SWE retrieval accuracy when compared to an assimilation scheme that requires in situ snow information [*Takala et al.*, 2011]. The *Takala et al.* [2011] study identified RMSE values ranging between 23 and 73 mm over Eurasia (depending on the season) and between 21 and 70 mm over Canada (depending on land cover).

[40] In this study, we covered a wide range of measurements from very low values that can be expected in the fall to high values expected at the end of winter. Furthermore, we covered an extensive area ($>$2000 km) encompassing several environments (boreal, taiga, tundra) with specific physical processes governing snow accumulation and transport. This said, with proper assessment of the various contributions to T_b (i.e., topography, vegetation, atmosphere), we believe the data set to be representative of subarctic regions and that the method and threshold can be regionally applied. Prior to doing so, the next intuitive step would be to extend the validation of the method using a multiscale (in situ, airborne, spaceborne) approach. The differences in errors observed at the various scales using the same field SWE reference measurements averaged at the different scales will explain the potential source of errors at the satellite scale. The proposed simplified approach could also be applied regionally with a snow model or within the land surface scheme of a regional climate model to potentially improve snow monitoring. Furthermore, the physical processes driving the initial SNOWPACK model biases in SWE such as precipitation parameterization, treatment of albedo and density (starting values and temporal evolution), sublimation/erosion, and their seasonal evolution should be addressed in a dedicated study.

[41] **Acknowledgments.** The authors thank the Churchill Northern Studies Centre and Environment Canada staff that participated in the project for their collaboration and support. The authors acknowledge the generous contributions of G. Picard, L. Arnaud, L. Brucker, N. Champollion, J.-D. Giguère, A. Roy, S. Crête-d'Avignon, C. Rivest, M. Chum, P. Harvey-Collard, and S. Langlois for helping to collect the data in harsh arctic winter conditions. Special thanks to Peter Toose and Arvids Silis from Environment Canada, M. Dufour, and Heli-Excel for making the ambitious helicopter transect possible and to the McGill Subarctic Research Station and Makivik Corporation staff for essential logistical support. This project was funded through the Canadian IPY project-Environment Canada, the National Sciences and Engineering Research Council of Canada, the Collaboration Québec-France, Le Centre Jacques Cartier and the French Remote Sensing program (Programme National de Télédétection Spatiale), and the Canadian Space Agency.

References

Albert, M. R. (2002), Effects of snow and firn ventilation on sublimation rates, *Ann. Glaciol.*, *35*, 510–514.

Andreadis, K., and D. Lettenmaier (2006), Trends in 20th century drought over the continental United States, *Geophys. Res. Lett.*, *33*, L10403, doi:10.1029/2006GL025711.

Arons, E. M., and S. C. Colbeck (1995), Geometry of heat and mass transfer in dry snow: A review of theory and experiment, *Rev. Geophys.*, *33*, 463–493.

Asmus, K., and C. Grant (1999), Surface based radiometer (SBR) data acquisition system, *Int. J. Remote Sens.*, *20*, 3125–3129.

Barnett, T. P., J. C. Adam, and D. P. Lettenmaier (2005), Potential impacts of a warming climate on water availability in snow-dominated regions, *Nature*, *438*, 303–309, doi:10.1038/nature04141.

Bartelt, P. B., and M. Lehning (2002), A physical SNOWPACK model for avalanche warning services. Part I: Numerical model, *Cold Reg. Sci. Technol.*, *35*(3), 123–145.

Brown, R. D., B. Brasnett, and D. Robinson (2003), Gridded North American monthly snow depth and snow water equivalent for GCM evaluation, *Atmos. Ocean*, *41*, 1–14.

Brucker, L., A. Royer, G. Picard, A. Langlois, and M. Fily (2010), Hourly simulations of seasonal snow microwave brightness temperature using coupled snow evolution-emission models in Québec, Canada, *Remote Sens. Environ.*, *115*, 1966–1977.

Bukovsky, M. S., and D. J. Karoly (2007), A brief evaluation of precipitation from the North American regional reanalysis, *J. Hydrometeorol.*, *8*(4), 837–847.

Butt, M., and R. E. J. Kelly (2008), Monitoring snowcover in the UK using passive microwave remote sensing observations and the HUT model, *Int. J. Remote Sens.*, *29*(14), 4249–4267, doi:10.1080/01431160801891754.

Chang, A. T. C., J. L. Foster, D. K. Hall, A. Rango, and B. K. Hartline (1982), Snow water equivalent estimation by microwave radiometry, *Cold Reg. Sci. Technol.*, *5*(3), 259–267.

Clark, M. P., J. Hendrikx, A. G. Slater, D. Kavetski, B. Anderson, N. J. Cullen, T. Kerr, E. Örn Hreinsson, and R. A. Woods (2011), Representing spatial variability of snow water equivalent in hydrologic and land-surface models: A review, *Water Resour. Res.*, *47*, W07539, doi:10.1029/2011WR010745.

Colbeck, S. C. (1983), Theory of metamorphism of dry snow, *J. Geophys. Res.*, *88*, 5475–5482.

Derksen, C., A. Walker, and B. Goodison (2005), Evaluation of passive microwave snow water equivalent retrievals across the boreal forest/tundra transition of western Canada, *Remote Sens. Environ.*, *96*(3–4), 315–327.

Derksen, C., P. Toose, A. Rees, L. Wang, M. English, A. Walker, and M. Sturm (2010), Development of a tundra-specific snow water equivalent retrieval algorithm for satellite passive microwave data, *Remote Sens. Environ.*, *114*, 1699–1709.

Derksen, C., P. Toose, J. Lemmetyinen, J. Pulliainen, A. Langlois, N. Rutter, and M. Fuller (2012a), Evaluation of passive microwave brightness temperature simulations and snow water equivalent retrievals through a winter season, *Remote Sens. Environ.*, *117*, 236–248.

Derksen, C., et al. (2012b), Variability and change in the Canadian cryosphere, *Clim. Change*, *115*, 59–88, doi:10.1007/s10584-012-0470-0.

Domine, F., R. Salvatori, L. Legagneux, R. Salzano, M. Fily, and R. Casacchia (2006), Correlation between the specific surface area and the short wave infrared (SWIR) reflectance of snow, *Cold Reg. Sci. Technol.*, *46*, 60–68.

Domine, F., M. Albert, T. Huthwelker, H.-W. Jacobi, A. A. Kokhanovsky, M. Lehning, G. Picard, and W. R. Simpson (2008), Snow physics as relevant to snow photochemistry, *Atmos. Chem. Phys.*, *8*, 171–208.

Dong, J., J. P. Walker, and P. R. Houser (2005), Factors affecting remotely sensed snow water equivalent uncertainty, *Remote Sens. Environ.*, *97*(1), 68–82.

Durand, M., and S. A. Margulis (2007), Correcting first-order errors in snow water equivalent estimates using a multifrequency, multiscale radiometric data assimilation scheme, *J. Geophys. Res.*, *112*, D13121, doi:10.1029/2006JD008067.

Durand, M., E. J. Kim, and S. A. Margulis (2008), Quantifying uncertainty in modeling snow microwave radiance for a mountain snowpack at the point-scale, including stratigraphic effects, *IEEE Trans. Geosci. Remote Sens.*, *46*(6), 1753–1767.

Dutra, E., G. Balsamo, P. Viterbo, P. M. A. Miranda, A. Beljaars, C. Schär, and K. Elder (2010), An improved snow scheme for the ECMWF land surface model: Description and offline validation, *J. Hydrometeorol.*, *11*(4), 899–916, doi:10.1175/2010JHM1249.1.

Essery, R. (1998), Boreal forests and snow in climate models, *Hydrol. Process.*, *12*(10–11), 1561–1567.

Fletcher, C. G., P. J. Kushner, A. Hall, and X. Qu (2009), Circulation responses to snow albedo feedback in climate change, *Geophys. Res. Lett.*, *36*, L09702, doi:10.1029/2009GL038011.

Foster, J. L., A. T. C. Chang, and D. K. Hall (1997), Comparison of snow mass estimates from a prototype passive microwave snow algorithm, a revised algorithm and a snow depth climatology, *Remote Sens. Environ.*, *62*, 132–142.

Foster, J. L., C. Sun, J. P. Walker, R. Kelly, A. T. C. Chang, J. Dong, and H. Powell (2005), Quantifying the uncertainty in passive microwave snow water equivalent observations, *Remote Sens. Environ.*, *94*(2), 187–203.

Foster, J. L., et al. (2011), A blended global snow product using visible, passive microwave and scatterometer satellite data, *Int. J. Remote Sens.*, *32*(5), 1371–1395.

Frei, A., and S. Lee (2010), A comparison of optical-band based snow extent products during spring over North America, *Remote Sens. Environ.*, *114*, 1940–1948.

Gallet, J.-C., F. Domine, C. S. Zender, and G. Picard (2009), Measurement of the specific surface area of snow using infrared reflectance in an integrating sphere at 1310 and 1550 nm, *Cryosphere*, *3*, 167–182.

Gallet, J.-C., F. Domine, L. Arnaud, G. Picard, and J. Savarino (2010), Vertical profiles of the specific surface area of the snow at Dome C, Antarctica, *Cryosphere Discuss.*, *4*, 1647–1708.

Grenfell, T. C., and S. G. Warren (1999), Representation of a nonspherical ice particle by a collection of independent spheres for scattering and absorption of radiation, *J. Geophys. Res.*, *104*, 31,697–31,708.

Grody, N. (2008), Relationship between snow parameters and microwave satellite measurements: Theory compared with Advanced Microwave Sounding Unit observations from 23 to 150 GHz, *J. Geophys. Res.*, *113*, D22108, doi:10.1029/2007JD009685.

Gustafsson, D., M. Stähli and P.-E. Jansson (2001), The surface energy balance of a snow cover: Comparing measurements to two different simulation models, *Theor. Appl. Climatol.*, *70*, 81–96.

Hall, D. K., G. A. Riggs, and V. V. Salomonson (1995), Development of methods for mapping global snow cover using moderate resolution imaging spectroradiometer data, *Remote Sens. Environ.*, *54*, 27–140.

Hallikainen, M., F. T. Ulaby, and M. Abdelrazik (1986), Dielectric properties of snow in the 3 to 37 GHz range, *IEEE Trans. Ant. Propag.*, *34*, 1329–1340.

Hansen, M., R. DeFries, J. R. G. Townshend, R. Sohlberg, C. Dimiceli, and M. Carroll (2002), Towards an operational MODIS continuous fields of percent tree cover algorithm: Example using AVHRR and MODIS data, *Remote Sens. Environ.*, *83*, 303–319.

Hardiman, S. C., P. J. Kushner, and J. Cohen (2008), Investigating the ability of general circulation models to capture the effects of Eurasian snow cover on winter climate, *J. Geophys. Res.*, *113*, D21123, doi:10.1029/2008JD010623.

Huang, C., S. A. Margulis, M. T. Durand, and K. N. Musselman (2012), Assessment of snow grain-size model and stratigraphy representation impacts on snow radiance assimilation: Forward modeling evaluation, *IEEE Trans. Geosci. Remote Sens.*, *50*, 4551–4561, doi:10.1109/TGRS.2012.2192480.

Huining, W., J. Pulliainen, and M. Hallikainen (1999), Effective permittivity of dry snow in the 18 to 90 GHz range, *Prog. Electromagn. Res.*, *24*, 119–138.

Kaufman, D. S., et al. (2009), Recent warming reverses long-term Arctic cooling, *Science*, *325*(5945), 1236–1239.

Kelly, R., A. T. C. Chang, L. Tsang, and J. Foster (2003), A prototype AMSR-E global snow area and snow depth algorithm, *IEEE Trans. Geosci. Remote Sens.*, *41*(2), 230–242.

Kerr, Y. H., and E. G. Njoki (1990), A semiempirical model for interpreting microwave emission from semiarid land surfaces as seen from space, *IEEE Trans. Geosci. Remote Sens.*, *28*(3), 384–393.

Kontu, A., and J. Pulliainen (2010), Simulation of spaceborne microwave radiometer measurements of snow cover using in situ data and brightness temperature modeling, *IEEE Trans. Geosci. Remote Sens.*, *48*(3), 1031–1044.

Kruopis, N., J. Praks, A. N. Arslan, H. Alasalmi, J. Koskinen, and M. Hallikainen (1999), Passive microwave measurements of snow-covered forest areas in EMAC'95, *IEEE Trans. Geosci. Remote Sens.*, *37*(6), 2699–2705.

Langlois, A., D. G. Barber, and B. J. Hwang (2007), Development of a snow water equivalent algorithm using passive microwave data over first-year sea ice, *Remote Sens. Environ.*, *106*(1), 75–88.

Langlois, A., T. Fisico, D. G. Barber, and T. N. Papakyriakou (2008), The response of snow thermophysical processes to the passage of a polar low-pressure system and its impact on in-situ passive microwave data: A case study, *J. Geophys. Res.*, *113*, C03S04, doi:10.1029/2007JC004197.

Langlois, A., L. Brucker, J. Kohn, A. Royer, C. Derksen, P. Cliche, G. Picard, M. Fily, and J.-M. Willemet (2009), Regional retrieval of snow water equivalent (SWE) using thermodynamic snow models in Québec, Canada, *J. Hydrometeorol.*, *10*(6), 1447–1463.

Langlois, A., A. Royer, and K. Goïta (2010a), Linkages between simulated and spaceborne passive microwave brightness temperatures with in-situ measurements of snow and vegetation properties, *Can. IPY Spec. Issue Can. J. Remote Sens.*, *36*(1), 135–148.

Langlois, A., A. Royer, B. Montpetit, G. Picard, L. Brucker, L. Arnaud, K. Goïta, and M. Fily (2010b), On the relationship between measured and modeled snow grain morphology using infrared reflectance, *Cold Reg. Sci. Technol.*, *61*, 34–42.

Langlois, A., A. Royer, F. Dupont, A. Roy, K. Goïta, and G. Picard (2011), Improved vegetation corrections for satellite passive microwave remote sensing using airborne radiometer data, *IEEE Trans. Geosci. Remote Sens.*, *49*(10), 3824–3837.

Latifovic, R., Z.-L. Zhu, J. Cihlar, C. Giri, and I. Olthof (2004), Land cover mapping of North and Central America—Global land cover 2000, *Remote Sens. Environ.*, *89*(1), 116–127.

Lehning, M., P. B. Bartelt, R. L. Brown, C. Fierz, and P. Satyawali (2002), A physical SNOWPACK model for the Swiss Avalanche Warning Services. Part III: Meteorological boundary conditions, thin layer formulation and evaluation, *Cold Reg. Sci. Technol.*, *35*(3), 169–184.

Lemke, P., et al. (2007), Observations: Changes in snow, ice and frozen ground, in: Climate Change 2007: The Physical Science Basis, in *Contribution of Working Group I to the Fourth Assessment Report of the Intergovernmental Panel on Climate Change*, edited by S. Solomon, et al., Cambridge Univ. Press, New York.

Lemmetyinen, J., C. Derksen, J. Pulliainen, W. Strapp, P. Toose, A. Walker, S. Tauriainen, J. Pihlflyckt, J.-P. Kärnä, and M. T. Hallikainen (2009), A comparison of airborne microwave brightness temperatures and snowpack properties across the boreal forests of Finland and Western Canada, *IEEE Trans. Geosci. Remote Sens.*, *47*(3), 965–978.

Li, S., and X. Zhou (2001), Derivation of surface direct beam spectral albedo for a wide range of incident angles from spectral reflectance measurements under overcast conditions, paper presented at IEEE 2001 International Geoscience and Remote Sensing Symposium (IGARSS 2001), Sydney, Australia, 9–13 July, pp. 1801–1803.

Lundy, C. C. (2000), Statistical validation of a numerical snow cover model and preliminary experimental results to facilitate model improvement, M.Sc. thesis, Dept. Civil. Eng., Mont. State Univ., Bozeman, Mont.

Male, D. H., and R. J. Granger (1981), Snow surface energy exchange, *Water Resour. Res.*, *17*, 609–627.

Markus, T., and D. Cavalieri (2000), An enhancement of the NASA Team Sea Ice Algorithm, *IEEE Trans. Geosci. Remote Sens.*, *38*, 1387–1398.

Markus, T., D. C. Powell, and J. R. Wang (2006), Sensitivity of passive microwave snow depth retrievals to weather effects and snow evolution, *IEEE Trans. Geosci. Remote Sens.*, *44*, 68–77.

Matzl, M., and M. Schneebeli (2006), Areal measurement of specific surface area in snow profiles by near infrared reflectivity, *J. Glaciol.*, *52*(179), 558–564.

Mätzler, C. (1987), Applications of the interaction of microwaves with natural snow cover. *Remote Sens. Rev.*, *2*(1), 259–387.

Mätzler, C. (1992a), Relation between grain-size and correlation length of snow, *J. Glaciol.*, *48*(162), 461–466.

Mätzler, C. (1992b), Ground-based observations of atmospheric radiation at 5, 10, 21, 35, and 94 GHz, *Radio Sci.*, *27*(3), 403–415.

Mätzler, C., and A. Wiesmann (1999), Extension of the microwave emission model of layered snowpacks to coarse-grained snow, *Remote Sens. Environ.*, *70*(3), 317–325.

Maurer, E. P., J. D. Rhoads, R. O. Dubayah, and D. P. Lettenmaier (2003), Evaluation of the snow-covered area data product from MODIS, *Hydrol. Process.*, *17*, 59–71.

Mesinger, F., et al. (2006), North American Regional Reanalysis, *Bull. Am. Meteorol. Soc.*, *87*(3), 343–360.

Metcalfe, J. R., and B. E. Goodison (1993), Correction of Canadian winter precipitation data, paper presented at Eighth Symposium on Meteorological Observations and Instrumentation, Anaheim, Calif., AMS, Boston, Mass.

Montpetit, B., A. Royer, A. Langlois, P. Cliche, A. Roy, N. Champollion, G. Picard, F. Domine, and R. Obbard (2011), New short-wave infrared albedo measurements for snow specific surface area retrieval, *J. Glaciol.*, *58*, 941–952.

Morin, S., F. Domine, A. Dufour, Y. Lejeune, B. Lesaffre, J.-M. Willemet, C. M. Carmagnola, and H.-W. Jacobi (2012), Measurements and modeling of the vertical profile of specific surface area of an alpine snowpack, *Adv. Water Resour.*, doi:10.1016/j.advwatres.2012.01.010, in press.

Pampaloni, P. (2004), Microwave radiometry of forests, *Waves Random Complex Medium*, *14*, 275–298.

Pardé, M., K. Goïta, A. Royer, and F. Vachon (2005), Boreal forest transmissivity in the microwave domain using ground-based measurements, *IEEE Trans. Geosci. Remote Sens.*, *2*(2), 169–171.

Pardé, M., K. Goïta, and A. Royer (2007), Inversion of a passive microwave snow emission model for water equivalent estimation using airborne and satellite data, *Remote Sens. Environ.*, *111*, 346–356.

Picard, G., L. Arnaud, F. Domine, and M. Fily (2010), Determining snow specific surface area from near-infrared reflectance measurements: Numerical study of the influence of grain shape, *Cold Reg. Sci. Technol.*, *56*, 10–17.

Pulliainen, J. (2006), Mapping of snow water equivalent and snow depth in boreal and sub-arctic zones by assimilating space-borne microwave radiometer data and ground-based observations, *Remote Sens. Environ.*, *101*(2), 257–269.

Pulliainen, J., and M. Hallikainen (2001), Retrieval of regional snow water equivalent from space-borne passive microwave observations, *Remote Sens. Environ.*, *75*(1), 76–85.

Qiu, Y., H. Guo, J. Shi, S. Kang, J. Lemmetyinen, and J. R. Wang (2011), Analysis of the passive microwave high-frequency signal in the shallow snow retrieval, in *Geoscience and Remote Sensing Symposium (IGARSS), 2011*, IEEE International, 24–29 July 2011, pp. 3863–3866.

Rees, A., J. Lemmetyinen, C. Derksen, J. Pulliainen, and M. English (2010), Observed and modelled effects of ice lens formation on passive microwave brightness temperatures over snow covered tundra, *Remote Sens. Environ.*, *114*, 116–126.

Romanovsky, V. E., S. L. Smith, and H. H. Christiansen (2010), Permafrost thermal state in the polar northern hemisphere during the International Polar Year 2007–2009: A synthesis, *Permafrost Periglacial Process.*, *21*(2), 106–116.

Rosenfeld, S., and N. Grody (2000), Anomalous microwave spectra of snow cover observed from special sensor microwave/imager measurements, *J. Geophys. Res.*, *105*(D11), 14,913–14,925.

Roy, V., K. Goïta, A. Royer, A. Walker, and B. Goodison (2004), Snow water equivalent retrieval in a Canadian boreal environment from microwave measurements using the HUT snow emission model, *IEEE Trans. Geosci. Remote Sens.*, *42*(9), 1850–1859.

Salomonson, V. V., and I. Appel (2004), Estimating fractional snow cover from MODIS using the normalized difference snow index, *Remote Sens. Environ.*, *89*, 351–360.

Shook, K., and D. M. Gray (1996), Small-scale spatial structure of shallow snowcovers, *Hydrol. Process.*, *10*, 1283–1292.

Solheim, F. 1993, Use of pointed water vapor radiometers to improve GPS surveying accuracy, Ph.D. dissertation, Univ. of Colo., Boulder, Colo., December.

Spreitzhofer, G., C. Fierz, and M. Lehning (2004), SN_GUI: A graphical user interface for snow pack modeling, *Comput. Geosci.*, *30*(8), 809–816.

Takala, M., K. Luojus, J. Pulliainen, C. Derksen, J. Lemmetyinen, J.-P. Kärnä, J. Koskinen, and B. Bojkov (2011), Estimating northern hemisphere snow water equivalent for climate research through assimilation of space-borne radiometer data and ground-based measurements, *Remote Sens. Environ.*, *115*(12), 3517–3529.

Tedesco, M., and E. J. Kim (2006), Intercomparison of electromagnetic models for passive microwave remote sensing of snow, *IEEE Trans. Geosci. Remote Sens.*, *44*(10–1), 2654–2666.

Tiuri, M. E., A. H. Sihlova, E. G. Nyfors, and M. T. Hallikainen (1984), The complex dielectric constant of snow at microwave frequencies, *IEEE J. Ocean. Eng.*, *9*(5), 377–382.

Touré, A. M., K. Goïta, A. Royer, E. J. Kim, M. Durand, S. A. Margulis, and H. Lu (2011), A case study of using a multilayered thermodynamical snow model for radiance assimilation, *IEEE Trans. Geosci. Remote Sens.*, *49*(8), 2828–2837.

Walker, A., J. W. Strapp, and I. MacPherson. (2002) A Canadian Twin Otter microwave radiometer installation for airborne remote sensing of snow, ice and soil moisture, paper presented at International Geoscience and Remote Sensing Symposium [CD-ROM], Toronto, Ont., June.

Wegmüller, U., and C. Mätzler (1999), Rough bare soil reflectivity model, *IEEE Trans. Geosci. Remote Sens.*, *37*(3), 1391–1395.

Wiesmann, A., and C. Mätzler (1999), Microwave emission model of layered snowpacks, *Remote Sens. Environ.*, *70*(3), 307–316.

Wiesmann, A., C. Mätzler, and T. Weise (1998), Radiometric and structural measurements of snow samples, *Radio Sci.*, *33*(2), 273–289.

Yang, D., S. Ishida, B. E. Goodison, and T. Gunther (1999), Bias correction of daily precipitation for Greenland, *J. Geophys. Res.*, *104*(D6), 6171–6181.